Earth and Planetary Science Letters 609 (2023) 118101

Contents lists available at ScienceDirect

Earth and Planetary Science Letters

journal homepage: www.elsevier.com/locate/epsl

Indian margin methane hydrate dissociation recorded in the carbon isotopes of benthic (Miliolida) foraminifera

S.C. Clemens [a,*], K. Thirumalai [a,b], D. Oppo [c]

[a] Earth Environmental and Planetary Sciences, Brown University, Providence, RI, USA
[b] Department of Geosciences, The University of Arizona, Tucson, AZ, USA
[c] School of Geosciences, The University of Louisiana at Lafayette, Lafayette, LA, USA

ARTICLE INFO

Article history:
Received 9 August 2022
Received in revised form 10 February 2023
Accepted 28 February 2023
Available online xxxx
Editor: L. Coogan

Keywords:
methane hydrate
Miliolida foraminifera
Pyrgo
Spiroloculina
Quinqueloculina
IODP Site U1446
Mahanadi basin
Bay of Bengal

ABSTRACT

Methane hydrates in ocean sediments have been investigated across various timescales using a broad array of indicators to better understand hydrate dynamics and climate linkages. Here we report individual benthic and planktonic foraminiferal isotopic analyses at three sites from distinct oceanic environments in the northern Indian Ocean. The multi-species, multi-site analyses identify a unique $\delta^{13}C$ response in Miliolida benthic foraminifera *Pyrgo* spp., *Quinqueloculina* spp., and *Spiroloculina* spp. suggesting that some species within these genera record the location and timing of past methane hydrate dissociation in the stable carbon isotopic composition of their skeletal (test) material. Our results document that dissociation occurred in the Mahanadi offshore basin, northwest Bay of Bengal, during glacial, transitional, and interglacial intervals of the past 1.5 million years. More negative test $\delta^{13}C$ coupled with more positive $\delta^{18}O$ supports the inference of interglacial-age dissociation, likely driven by increased intermediate water temperatures.

1. Introduction

Methane (CH_4) is a greenhouse gas (IPCC, 2021) for which the magnitude of its transfer from the global ocean to the atmosphere over time remains unclear. Current estimates indicate that seafloor methane seepage contributes less than ~2% of modern atmospheric methane (Ruppel and Kessler, 2017). Nevertheless, the contribution may have been greater at times in the geological past (Oppo et al., 2020), in particular when associated with gas hydrate dissociation (Dickens et al., 1995; Kennett et al., 2000; Kim and Zhang, 2022). The development of future global climate change scenarios will benefit from an enhanced understanding of past and present forcings governing oceanic methane dynamics {e.g. (Thirumalai et al., 2020)}.

Ongoing research seeks to identify locations and timing of hydrate dissociation activity, with the ultimate goal of better understanding mechanisms of hydrate instability and feedbacks related to climate change. Paleo-seep and -hydrate dissociation events have been identified in ocean sediment cores using several indicators, including sedimentological structures (Ma et al., 2021), authigenic carbonate and barite precipitates (Babineaux et al., 2021; Dickens et al., 2003; Lein, 2004; Teichert et al., 2014), and information derived from macro- and micro-biotic data (Åström et al., 2020; Lobegeier and Sen Gupta, 2008; Mazumdar et al., 2018; Sasaki et al., 2010; Sibuet and Roy, 2003).

The dissociation of methane hydrate has been studied at numerous locations worldwide, from equatorial to polar regions (Capozzi et al., 2012; Crutchley et al., 2013; Fang et al., 2019; Gieskes et al., 2011; Klaucke et al., 2010; Mazumdar et al., 2018; Melaniuk et al., 2022; Miller et al., 2015; Oppo and Hovland, 2019; Sassen et al., 1993; Wang et al., 2019). Methane input to the atmosphere is bio-regulated (Joye, 2020) by its microbial oxidation, including sulfate-driven anaerobic oxidation of methane (AOM) in the sediment column (Ruppel and Kessler, 2017) and aerobic oxidation of methane (MOx) in both the sediment and water columns (Hanson and Hanson, 1996; James et al., 2016). These processes drive increased pore water alkalinity and dissolved inorganic carbon (DIC; HCO_3^-) in which the carbon carries the strongly negative isotopic values of the methane from which it is derived; on the order of −30 to −50‰ (Lorenson and Collett, 2018; Whiticar, 1999). This negative isotopic signal can be incorporated into the $CaCO_3$ skeletal (test) material of foraminifera; single-celled protists living in the surface waters (planktonic) as well as upon and within

* Corresponding author.
E-mail addresses: steven_clemens@brown.edu (S.C. Clemens), kaustubh@arizona.edu (K. Thirumalai), davide.oppo@louisiana.edu (D. Oppo).

https://doi.org/10.1016/j.epsl.2023.118101

the first few centimeters of seafloor sediments (benthic). While anomalously negative δ^{13}C of benthic foraminifera tests is a key indicator of past methane dissociation, there has been much discussion as to whether the signal is primary, incorporated during biomineralization when the organism is alive, or secondary, incorporated as a function of postmortem diagenesis via authigenic carbonate overgrowth on the test (Melaniuk et al., 2022; Panieri et al., 2016, 2017). Both paths provide evidence for the location of hydrate activity and in some cases, the timing as well.

Several previous studies have used negative foraminifera δ^{13}C anomalies (benthic and planktonic) as indicators of methane hydrate dissociation and incorporation of methane-derived carbon into the overlying water column. Kennett et al. (2000) reported anomalous δ^{13}C in benthic (~0.5 to −6‰) and planktonic (~0.5 to −4‰) foraminifera during interstadials of the past 60,000 years. Citing the lack of evidence for diagenetic overprinting (scanning electron microscopy; SEM), they inferred that temperature-mediated methane release from the shallow flank of the Santa Barbara basin (120 m) impacted both the sediments and the overlying water column. Hill et al. (2003) documented extremely negative planktonic (~ −0.1 to −22‰) and benthic (~ −0.01 to −25‰) δ^{13}C values in glacial-age sediments of the Santa Barbara Channel. Citing the lack of evidence for diagenetic overprinting (SEM), these authors also inferred that methane release impacted both the sediments and the overlying water column. Keigwin (2002) found planktonic (~1 to −6‰) and benthic (~ −0.5 to −3‰) δ^{13}C anomalies in Holocene sediments in the Gulf of California (818 m), inferring methane oxidation within the water column. Rathburn et al. (2003) observed benthic δ^{13}C anomalies (~0.5 to −5.5‰) in living specimens at a modern methane seep in Monterey Bay (~1000 m). Citing cleaning procedures and the unlikelihood of overgrowths on the skeletal components of living specimens, they attributed these anomalies to methane-influenced pore water DIC. Zhou et al. (2020) report planktonic δ^{13}C anomalies (~1.5 to −4‰) in an 808-cm piston core from the gas hydrate zone of the Nansha Trough (2796 m), South China Sea, interpreted as resulting from the assimilation of methane-derived DIC and indicative of methane emission events. Finally, Melaniuk et al. (2022) report values of −5.2‰ in live foraminifera tests and −6.5‰ in fossil tests recovered from aerobic and anaerobic sediments at Arctic methane hydrate seeps (1200 m). They inferred the incorporation of methane-derived carbon via feeding on methanotrophic bacteria and/or incorporation via methane-influenced DIC. In summary, these studies document methane-influenced benthic δ^{13}C excursions of −4 to −6‰ (with some as low as −25‰,) with overall low likelihood for diagenetic overprinting inferred via various methodologies.

In contrast, similar anomalies in late Pleistocene tests (to −25‰) have been attributed to post-depositional overgrowth of methane-derived authigenic carbonate (MDAC), associated with the sulfate to methane transition zone (SMTZ) (Day, 2003; Joshi et al., 2014; Martin et al., 2004; Portilho-Ramos et al., 2018; Rathburn et al., 2003; Ussler and Paull, 2008; Wan et al., 2018). These contrasting interpretations are, in part, motivated by the recognition that it is difficult to detect the small amount of authigenic carbonate (e.g., at −50‰) sufficient to alter initial test δ^{13}C (at ~0‰) by small but measurable amounts (Torres et al., 2010, 2003). In addition, studies of live benthic foraminifera at active methane seep environments indicate strong disequilibrium between the test δ^{13}C (0.5 to −5‰) and the strongly negative carbon isotopic values (−30 to −40‰) of pore waters they inhabit (Bernhard et al., 2010; Gieskes et al., 2011; Rathburn et al., 2003). Such observations have been used to infer that benthic foraminifera may calcify intermittently, possibly when methane venting is less active, or that calcifying individuals move to more ideal microhabitats, avoiding methane-influenced waters (Bernhard et al., 2010; McCorkle et al., 1990). These study sites are often in active seep environments characterized by methane bubbling from the seafloor, abundant authigenic micro and macro carbonate precipitates with strongly negative δ^{13}C values (~ −30 to −60‰), and endemic macro-fauna. Rathburn et al. (2003) recognized the difficulty in attributing anomalously low δ^{13}C specifically to biomineralized δ^{13}C, post-depositional overprinting with MDAC, or some combination thereof. They suggested that hydrate dissociation events in the sediment record can be identified by wide conspecific δ^{13}C ranges.

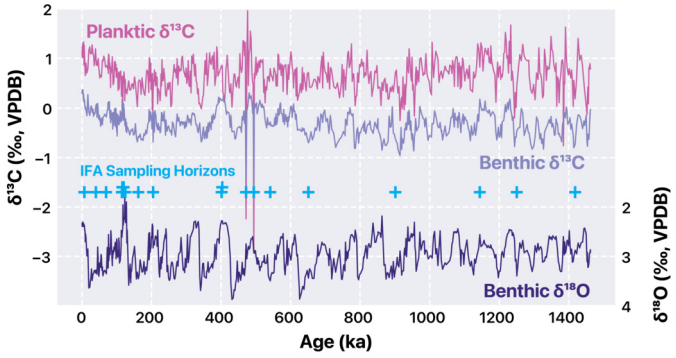

Fig. 1. U1446 stable isotope time series (Clemens et al., 2021) showing bulk planktonic (*G. ruber*) and benthic (*C. wuellerstorfi*) δ^{13}C anomalies in Marine Isotope Stage 13 (*U1446A 10H 3 33.5 cm, 35.5 cm and U1446C 9H 4, 39.5 cm*) as well as location of IFA samples (+). Benthic δ^{18}O shown to indicate glacial and interglacial variability.

As indicated above, the definition of what constitutes 'anomalous' varies among publications. Here 'anomalously negative' δ^{13}C is defined as values lower than those commonly associated with epifaunal to deep infaunal microhabitats in non-hydrate-impacted marine settings; that is, values more negative than ~ −2‰ {(McCorkle et al., 1990; Mulitza et al., 2022; Schneider et al., 2017) and references therein}. This threshold is also, in part, chosen on the basis of the clear anomalies revealed in the 1.46-million-year long time series of benthic and planktonic foraminifera δ^{13}C at the location we investigate, IODP Site U1446 (Fig. 1). δ^{13}C values are reported in permille (‰) relative to the Vienna Pee Dee Belemnite (VPDB) reference frame.

Here we investigate Pleistocene-age hydrate dissociation events in the Mahanadi Basin, northwest Bay of Bengal, as well as the utility of fossil Miliolida foraminifera test δ^{13}C as an indicator of the timing and location of hydrate dissociation. Our investigation conformed to the challenges described above; analysis of the best-preserved individuals, based on visual inspection of the whole test, was not diagnostic of anomalous δ^{13}C. This is confirmed by SEM observation of authigenic carbonate growth on the inner chamber relative to the outer test surface (Fig. 2a-c). Here, instead, we draw inferences using multi-species, multi-site individual foraminifera analyses (IFA). We present new benthic and planktonic δ^{13}C and δ^{18}O IFA results from three distinctly different environmental settings, including two non-hydrate-influenced control sites, Ninety East Ridge (open ocean pelagic) and northwest Arabian Sea (high productivity upwelling), and one hydrate-influenced site on the northeast Indian Margin (Fig. 3a). IFA of multiple benthic and planktonic species at these sites document the unique response of three benthic genera within the Miliolida order, only at the hemipelagic hydrate-influenced Indian margin, Site U1446. With the exception of samples from marine isotopic stage (MIS) 13, the anomalously negative δ^{13}C values within these three genera (to −17.5‰) are not recorded in other planktonic or benthic species from the same discrete sediment samples. In addition, no anomalies are found in foraminifera from the non-hydrate-influenced control sites within the upwelling and open-ocean pelagic regions. From these results we infer that species within these three Mil-

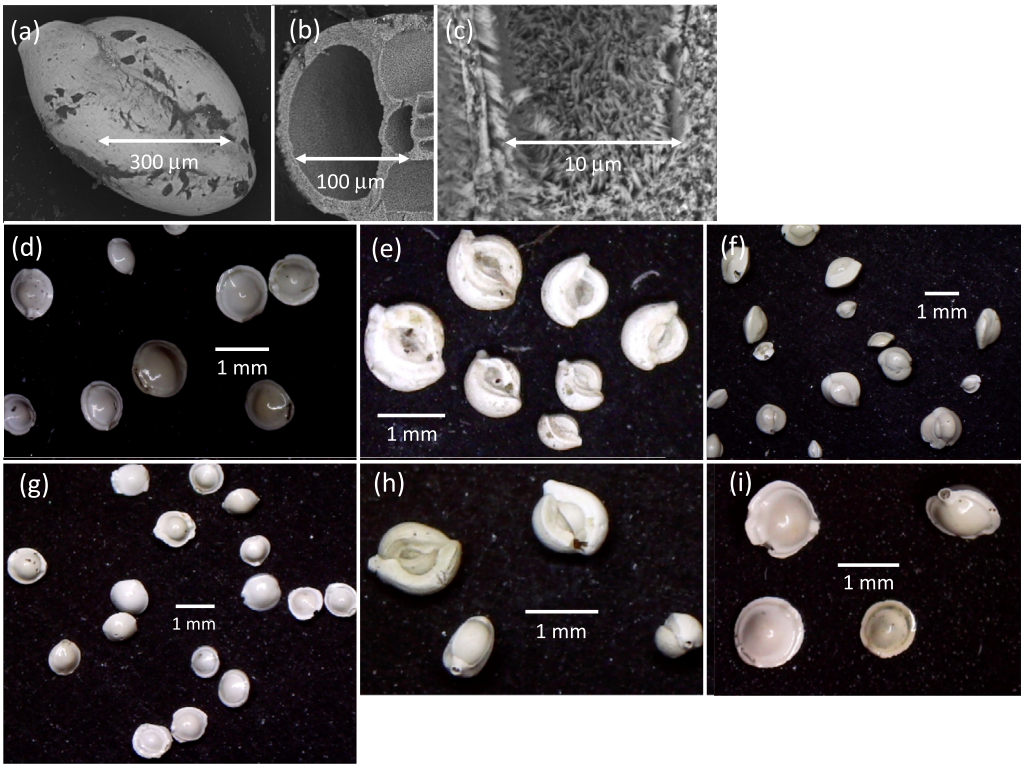

Fig. 2. U1446 Miliolida foraminifera. SEM photographs of *Quinqueloculina* sp. from U1446C-1H-4-50-52 cm (MIS1; IFA = −6.79‰ δ^{13}C VPDB) showing (a) the clean exterior test surface, (b) inner chambers of the broken test, and (c) authigenic carbonate overgrowths on the inner chamber wall. (d) *Pyrgo* spp. and (e) *Spiroloculina* sp. from U1446C-4H-5-145.5 cm (MIS 6). (f) Quinqueloculina spp., (g) *Pyrgo* spp., and (h) *Spiroloculina* sp. from U1446A-12H-3-6.5 (MIS 16). (i) *Pyrgo* spp. from U1446A-18H-7-81.5 (MIS 38).

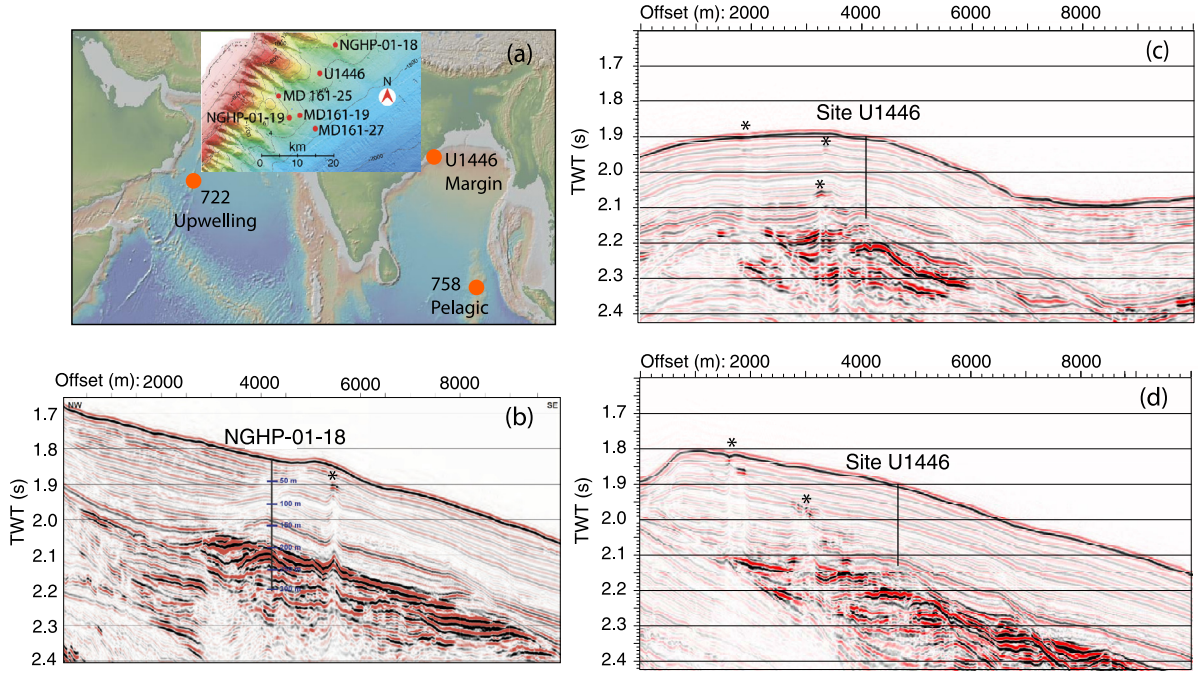

Fig. 3. Site locations and seismic sections. (a) Site locations. Inset shows site location bathymetry from ~600 mbsl (red) to 2000 mbsl (blue), after (Mazumdar et al., 2014). (b) NGHP-01-18 dip profile after Collett et al. (2015). (c) Site U1446 strike profile and (d) dip profile after Clemens et al. (2016b). Asterix denotes locations of gas escape pipes, the high-amplitude negative anomalies at the upper ends indicate low seismic velocity gas hydrate.

iolida genera are sensitive recorders of short-duration, transient hydrate dissociation events in the Mahanadi offshore basin; events insufficient to precipitate authigenic carbonate crusts and develop macro-biological communities at the seafloor. We find that such events occurred during glacial, transitional, and interglacial intervals within the past 1.4 million years. This is supported by higher test δ^{18}O coupled with lower test δ^{13}C during interglacial intervals, likely stemming from warming ocean temperatures.

2. Oceanographic and sedimentological settings

Site U1446 (19°5.01′N, 85° 44.08′E) is located in the Mahanadi offshore basin at 1430 m below sea level (mbsl) (Fig. 3a) (Clemens et al., 2016b). U1446 is at approximately the same depth and proximal to two sites drilled by the Indian National Gas Hydrate Program (NGHP); U1446 is ∼8 km southwest of NGHP-01-18 (1374 mbsl) and ∼14 km northeast of NGHP-01-19 (1422 mbsl) (Collett et al., 2015; Lorenson and Collett, 2018). Results from these two sites provide context for regional hydrate characteristics, based on analyses not conducted at U1446 (e.g., pressure coring, thermal imaging during core recovery etc.). Pleistocene sediments at U1446 are hemipelagic clays bearing nannofossils, foraminifera and minor amounts of biosilica, the same as at the NGHP sites but with more uniform seismic reflectors, selected for paleoclimate reconstructions (Fig. 3c, d). Sedimentation rates average 28±18 cm per kiloyear (cm/ky) over the past 250 thousand years (kyrs; 0 to 55 meters below sea floor - mbsf), decreasing to 13±4 cm/ky between 0.250 and 1.46 million years ago (55 to 204 mbsf). Each sample spanned two vertical cm, such that each one includes approximately 70 to 150 years of deposition, excluding bioturbation. Sedimentation rates at NGHP sites are poorly constrained; NGHP-01-19 rates are estimated at 10 cm/ky over the top 8 m and less than 4 cm/ky over the prior 2 million years (to ∼ 75 mbsf) (Collett et al., 2015). Total organic carbon content at U1446 ranges between 0.8 and 1.8 weight percent throughout the record (Clemens et al., 2016b), similar to that at NGHP-01-19 which varies between 0.9 and 1.3% over the 300 m long record (Johnson et al., 2014).

Reflection seismic sections at the three sites are characterized by seafloor-parallel or sub-parallel reflections down to ∼200 mbsf {∼0.2 seconds two-way travel time (TWT) with 2000 m/s average P-wave velocity}. Below this interval, there is an equal interval of high-amplitude reflectivity, the top of which likely represents the base of the gas hydrate stability zone (GHSZ), with free gas below (Collett et al., 2015). Seismic data shows vertical seismic anomalies nearby U1446 and NGHP-01-18 (Fig. 3b-d). These anomalies are interpreted as gas escape pipes according to well-established criteria {see, for example, (Oppo et al., 2021)}. The pipes' root zone is located below the inferred base of the GHSZ, and they terminate at various depths below the modern seafloor. The upper terminus is either a high-amplitude negative anomaly within the sediment {i.e., soft kick; (Brown, 2011)} indicating the presence of low seismic velocity in-situ gas hydrate (Collett et al., 2015) or a pockmark on the seafloor indicating the presence of free gas within the sediment and its vertical migration and expulsion at the seafloor. Analyses at the NGHP sites identified infrared (IR) cold anomalies at 55, 65, 115, and 180 mbsf (Collett et al., 2015) as well as pore-water freshening from 115 to 190 mbsf, suggesting the presence of disseminated, pore-filling gas hydrate at NGHP-01-18A (Collett et al., 2014). At NGHP-01-19A, IR measurements of the core liners at the time of recovery identified steadily decreasing temperature with depth to 205 mbsf, interpreted as indicative of disseminated gas hydrate (Collett et al., 2015). Analysis of well log resistivity data indicated hydrate presence in the 105-120 mbsf interval as well as gas hydrate estimated to occupy ∼15% of the pore space in 180-205 mbsf interval immediately above a bottom simulating reflector (BSR) (Collett et al., 2015, 2014). We infer broadly similar disseminated hydrates at U1446.

Headspace methane (CH_4) gas concentrations at U1446 increase between 30 and 80 meters, peaking at 1000 ppmv at 50 mbsf; (Clemens et al., 2016b). Similar peaks occur in the same depth range at NGHP-01-18 and NGHP-01-19 (Collett et al., 2015). Methane to ethane ratios and CH_4 $\delta^{13}C$ indicate the gas is of microbial origin, with CH_4 $\delta^{13}C$ ranging between −71 and −87‰ (mean of −74‰ VPDB) at the NGHP sites (Lorenson and Collett, 2018). Similarly, at U1446, the CH_4 $\delta^{13}C$ ranges between −70 and −98‰, with a mean of −78‰ VPDB (Peketi et al., 2020). $\delta^{13}C$ DIC at U1446 is −12.2‰ in the shallowest porewater sample measured (1.45-m below sea floor), decreasing to a minimum of −34.5‰ at 16.75 m (within the SMTZ at a sediment age of ∼74 Ka) and then increasing to ∼5‰ by 100 mbsf (Fig. 4).

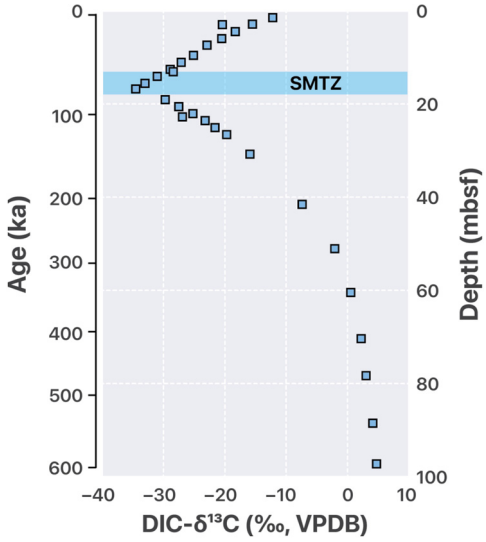

Fig. 4. Carbon isotope ratio of U1446 DIC indicating the current location of the SMTZ. After Peketi et al. (2020).

Pore-water profiles of sulfate, methane, alkalinity, ammonium and calcium from three nearby cores collected by R/V *Marion Dufresne* (MD; Fig. 3a) in the Mahanadi Basin between 1429 and 1691 m water depth are remarkably similar and are interpreted as dominantly influenced by anaerobic oxidation of methane (AOM) via AOM-induced sulfate consumption (Mazumdar et al., 2014). The SMTZ in these three cores occupy three- to four-meter thick zones centered on depths between 14 and 18 m below the sea floor (U1446 SMTZ is centered at 16.75 m). The pore-water profiles and shallow SMTZ, combined with hydrocarbon ratios and methane $\delta^{13}C$ analyses suggest that the methane is microbial in origin, with a high diffusive flux likely originating from the base of the gas hydrate stability zone (Mazumdar et al., 2014); we infer similar conditions for U1446.

Smear-slide analysis showed variable amounts of authigenic carbonate within the cored sediment at the NGHP sites. NGHP-01-18 showed trace-level to 4% authigenic carbonate in 6 of 49 samples dispersed throughout the core, none in the 43 coarse fraction (>63 microns) samples. Two authigenic carbonate nodules were documented; one in core 11H-2 at 85-95 cm (Collett et al., 2015) and one in 12H 4 85-87 cm (Babineaux et al., 2021; Dickens et al., 2003; Lein, 2004; Teichert et al., 2014). At NGHP-01-19, trace-level to 7% authigenic carbonate occur in 27 of 113 samples with one additional smear slide indicting 82% authigenic carbonate in core 10H-1, at 2 cm (Collett et al., 2015). Three carbonate nodules were identified and isotopically analyzed at NGHP-01-19, indicating clear methane-derived origins (Babineaux et al., 2021; Dickens et al., 2003; Lein, 2004; Teichert et al., 2014). The three nodules ranged from −28.5 to −41.9‰ $\delta^{13}C$. Smear slide analysis of U1446 identified authigenic carbonate ranging between 1 and 4% in 26 of 67 samples, with one sample reaching 10% in U1446A-17H-2, 4 cm (Clemens et al., 2016b). No authigenic carbonate nodules were identified in U1446.

On the basis of results described above at the nearby NGHP and MD sites, we infer the cored interval at U1446 to be within the modern gas hydrate stability zone with a high diffusive methane flux, of microbial origin, with the possibility of hydrates disseminated in low-concentrations within fine-grained sediments {Type-1

of You et al. (2019)}. We seek to assess the past variability in this system.

In this study, aside from the Indian Margin site, we also performed multi-species IFA at two other sites in the Indian Ocean, neither of which are hydrate influenced and serve as 'control' sites for comparison with U1446. ODP Site 722 lies atop the Owen Ridge, northwestern Arabian Sea (16° 37.312' N, 59° 47.755' E) at a water depth of 2028 m (Prell et al., 1989) (Fig. 3a). This site is characterized by strong upwelling and high productivity in response to summer-season southwest monsoon winds that drive upwelling of nutrient-rich waters into the photic zone from several hundred meters depth. Pleistocene sediments are composed of alternating light (interglacial) and dark (glacial) layers of foraminifer-bearing nannofossil ooze with sedimentation rates averaging ~4.5 cm/ky. ODP Site 758 lies atop the Ninetyeast Ridge (5°23.05′N, 90°21.67′E) at a water depth of 2924 m (Pierce et al., 1989). The location was recently drilled again, as Site U1443 (Clemens et al., 2016a). We analyzed Site 758 samples. Pleistocene sediments at this open ocean pelagic site are characterized by nannofossil ooze with varying proportions of foraminifers, clay, and volcanic ash with sedimentation rates averaging ~1.2 cm/ky.

3. Methods

Foraminifera stable carbon and oxygen isotope analyses were conducted on 290 samples from hemipelagic margin Site U1446, 39 from upwelling Site 722, and 52 from open ocean pelagic Site 758; all Late Pleistocene in age and including both glacial and interglacial intervals (Table S1). Samples were selected for analysis on the basis of the relatively high abundance of *Pyrgo* spp. in the >355 μm size fraction, having identified this genus as recording anomalously light δ^{13}C in interglacial MIS 13 of the time series record (Fig. 1). Given the limited supply of individuals large enough for IFA, we analyzed all species present, both pristine (visual assessment via binocular microscope) and visually degraded individuals (yellow tinted, sugary texture). In hindsight, it would have been useful to identify the individuals to the species level prior to analysis but this was not done in most cases. Sample preparation consisted of freeze-drying, wet-sieving (with 10% Calgon solution and sonification where necessary to move sediments through the sieves), rinsing in de-ionized water, and drying at 50 °C. IFA was conducted on the >355 μm fraction while bulk analysis (2 to 6 individuals) was conducted on the 250-355 μm fraction to test for differences in isotopic composition as a function of test size.

Analyses were conducted on either a MAT252 coupled to a Kiel III Carbonate Device (Brown University) or on a MAT 253+ coupled to Kiel IV Carbonate Device (Brown University and University of Arizona). Results are reported relative to ‰ VPDB with uncertainties of ±0.02 for δ^{13}C and ±0.04 for δ^{18}O of in-house BYM standard (n=16, 1σ) and ±0.03 for δ^{13}C and ±0.05 for δ^{18}O of in-house Carrara standard (n=34, 1σ).

4. Results

In the course of generating bulk planktonic and benthic foraminiferal stable isotope records for the reconstruction of U1446 seawater δ^{18}O (Clemens et al., 2021), two interglacial age δ^{13}C intervals within MIS 13 stood out as anomalously negative, in excess of 5 standard deviations from the mean (Fig. 1). These intervals were further investigated by 93 IFA on multiple species from MIS 13 (Fig. 5, Table S1). Anomalously negative δ^{13}C values are evident across both planktonic (to - 5.2‰) and benthic species (to −17.48‰), with anomalously wide conspecific δ^{13}C ranges (e.g. 7.1‰ for *Groborotalia menardii*, 2.24‰ *Neouvigerina proboscidea*, 2.08‰ *Globigerinoides sacculifer*), well beyond that expected for glacial- and interglacial-age variability. Notably, the carbon isotopic

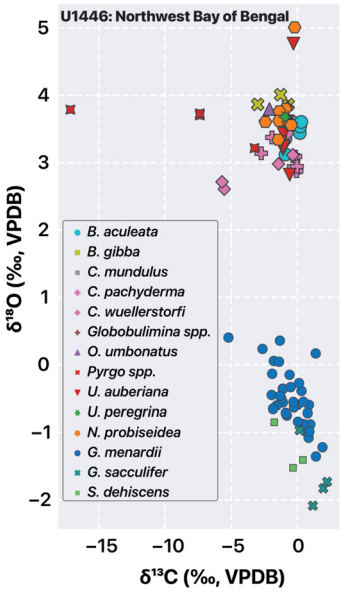

Fig. 5. U1446 MIS 13 IFA results documenting anomalously large ranges and anomalously negative δ^{13}C values of both benthic and planktonic species. MIS 13 samples are identified as anomalous in the time series records from Fig. 1. Refer to Table S1 for full genus names.

composition of *Pyrgo* spp. stands out, indicating strongly negative values extending to −17.1‰; far in excess of the most negative planktonic (−5.2‰) and benthic (−5.7‰) δ^{13}C values from other species in these MIS 13 samples.

An additional four glacial-age samples (from MIS 6, 14, 16, and 38), two transitional-age samples (from MIS 22-23 and 46–47), and 13 interglacial-age samples (from MIS 1, 3, 5, 7, 11, and 35) were investigated by 197 IFA of planktonic and benthic species to further assess the prevalence and timing of anomalous δ^{13}C events beyond those associated with MIS 13 (Table S1). Samples were chosen based on the abundance of *Pyrgo* in the >355-micron size fraction, allowing assessment of the range of anomalous IFA δ^{13}C. Intrasample Pyrgo δ^{13}C ranges from as large as 7.37‰ (MIS 46-47; n=13) to as small as 0.89‰ (MIS 6; n=6).

In addition to *Pyrgo*, we also assessed benthic species commonly utilized in paleoclimate studies including *Uvigerina* spp. and *Cibicidoides* spp. The results demonstrate an anomalously negative δ^{13}C response unique to genera within the Miliolida order including *Pyrgo* spp., *Spiroloculina* spp., and *Quinqueloculina* spp. (Fig. 2d-i, 6a, 7). For samples with abundant Pyrgo, IFA of large individuals (>355 μm) as well as bulk analyses on the smaller 250-355 μm fraction (2 to 6 individuals) showed no systematic difference in δ^{13}C anomalies (Fig. 7). Similarly, analysis of visually pristine (binocular microscope) versus visually degraded was not diagnostic of anomalously low δ^{13}C, consistent with findings described in the Introduction section.

The unique nature of the anomalous Miliolid δ^{13}C response was further investigated by IFA of glacial- and interglacial-age benthic and planktonic species from upwelling Site 722 and open-ocean pelagic Site 758. These control sites allow testing of the extent to which *Pyrgo* (available at all sites) is anomalous across a range of marine environments with differing sedimentation rates and organic carbon contents (Table S1, Fig. 6b, c). Anomalous δ^{13}C values documented at U1446 are not observed at either of the non-hydrate-influenced control sites.

5. Discussion

The basis for our choice of samples (abundant *Pyrgo*) does not appear to have biased the record; samples from glacial, interglacial,

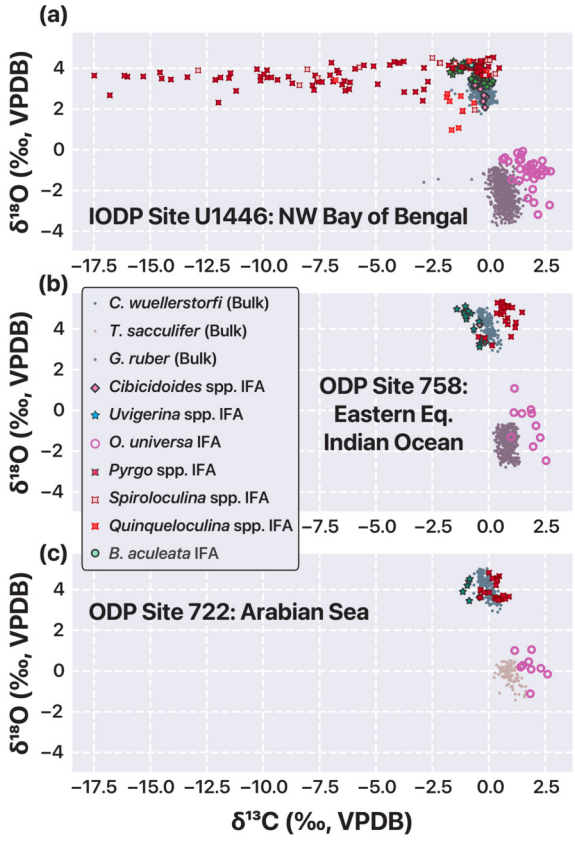

Fig. 6. IFA results from margin, pelagic, and upwelling environments. (a) U1446 IFA results from Indian margin samples with no anomalies in the time-series records of Fig. 1 (i.e. excluding MIS 13). Bulk planktonic and benthic data is from Clemens et al. (2021). (b) IFA results from pelagic Site 758 and (c) upwelling Site 722. Site 758 bulk planktonic and benthic data are from Bolton et al. (2013). Site 722 bulk planktonic and benthic data are from Clemens et al. (1996). Refer to Table S1 for full genus names.

and transitions between the two had sufficient *Pyrgo* at U1446. Both glacial- and interglacial-age samples were also available at the control sites. Samples investigated include MIS 11, 12, 15, and 16 at 758 and MIS 5 and MIS 6 at 722. The lowest *Pyrgo* δ^{13}C recorded were −0.46 and −0.38‰ at 758 and 722 respectively. The lowest values of any species at 758 and 722 were −1.41 and −1.15‰ respectively (both *Uvigerina*). Hence, anomalously low δ^{13}C values were not recorded at the non-hydrate-influenced control sites in the open ocean pelagic (758) or upwelling environment (722). This indicates that the anomalously low values recorded at U1446 are not endemic to the *Pyrgo* genus; they are inferred to be unique to the hydrate-influenced Indian margin environment.

The primary results requiring explanation at the U1446 Indian margin site are illustrated in Fig. 7, including: (1) the two MIS 13 samples with anomalous δ^{13}C recorded by all species (benthic and planktonic) relative to all other samples where only benthic Miliolida record anomalous values and (2) the anomalous benthic Miliolid δ^{13}C response relative to that of other benthic and planktonic individuals within the same discrete samples. We hypothesize that the observed relationships can be explained in the context of MDAC precipitation at the SMTZ (Ussler and Paull, 2008), upward movement of the SMTZ within the sediment column during hydrate dissociation events (Ruppel and Waite, 2020), and differences in ecological habitat and/or test structure of the Miliolida foraminifera.

5.1. Anomalous planktonic and benthic foraminifera δ^{13}C in MIS 13

Anomalous bulk foraminifera δ^{13}C values found in MIS 13 of the time-series record (Fig. 1) are also expressed in IFA of both benthic and planktonic species from these samples (Fig. 5). With the exception of *Pyrgo* spp., the anomalies range to −5.2‰ in the planktonic species (*Globorotalia menardii*) and −5.7‰ in the benthic species (*Cibicidoides wuellerstorfi*). In contrast, the δ^{13}C of *Pyrgo* spp. has strongly negative values, extending to −17‰, well outside the most negative planktonic and benthic δ^{13}C values of other species in the same samples. We interpret the anomalous δ^{13}C of benthic and planktonic species within the same sample as diagenetic in nature, likely via post-burial MDAC overgrowth (Wan et al., 2018).

This interpretation is consistent with similar findings at other hydrate-influenced sites. Day (2003) documents strongly negative benthic δ^{13}C values at the Eel River sites (520 m water depth, offshore California). Sediments at these sites were sampled by push cores (∼ 30 cm total length) during submersible dives. Eel River sites are active seeps, with gas bubbling, visible authigenic carbonate crusts and chimneys, cold-seep macrofauna and bacterial mats. At the Eel River location, all three benthic species analyzed showed extremely negative δ^{13}C, to −23‰ (Fig. 8). SEM examination yielded some evidence of authigenic carbonate precipitation and overprinting by authigenic carbonate was also inferred based on model-derived porewater saturation indices and the alteration of all species present. Panieri et al. (2009) document similar results for Miocene formations in the Northern Apennines. Again, all species evaluated had anomalously low δ^{13}C values (−9.04 to −25.74‰), and were interpreted in the context of overprinting with MDAC.

The results from Eel River (active) and Apennine (fossil) seep sites are similar to those of the U1446 MIS 13 samples, where all species analyzed were impacted. However, at U1446 there is no evidence of carbonate crusts, chimneys, or cold-seep macrobiological communities, with the possible exception of a single ∼3 cm scaphopod shell (U1446C 4H 7 34-37 cm, 37.786 mbsf, ∼179 Ka). As such, we interpret the δ^{13}C anomalies as linked to the disassociation of disseminated hydrates, as at nearby NGHP-01-19A (Collett et al., 2015). The extensive nature of the alteration (to −17‰) and the fact that both benthic and planktonic tests were impacted is interpreted to indicate that MDAC overprinting took place over some interval of time between MIS 13 and the present, when the SMTZ was stationary for an extended period at the location of the MIS 13 sediment layer. While the MIS 13 δ^{13}C results are consistent with the Eel River and Apennine sites as described, IFA results from the remaining 18 U1446 samples differ significantly in that only three benthic genera within the Miliolida order are impacted.

5.2. Anomalous δ^{13}C values only in Miliolida

In contrast to the two MIS 13 samples, the 18 other U1446 samples investigated show anomalous δ^{13}C only in three genera within the Miliolida order and not in any of the other planktonic or benthic foraminiferal species analyzed from the same samples (Fig. 7). Anomalous δ^{13}C was recorded only in *Pyrgo* spp., *Spiroloculina* spp., and *Quinqueloculina* spp. Species within the *Pyrgo* and *Quinqueloculina* genera have been reported in living populations beneath microbial mats at active Gulf of Mexico seep sites (Robinson et al., 2004) and are deep infaunal, having been observed as deep as 3 to 5 cm below the sea floor (Buzas et al., 1993; Enge et al., 2012; Gooday et al., 2010; Linke and Lutze, 1993).

The unique δ^{13}C response of these Miliolida, relative to other benthic and planktonic individuals from the same samples, may be explained by a combination of habitat and/or shell structure

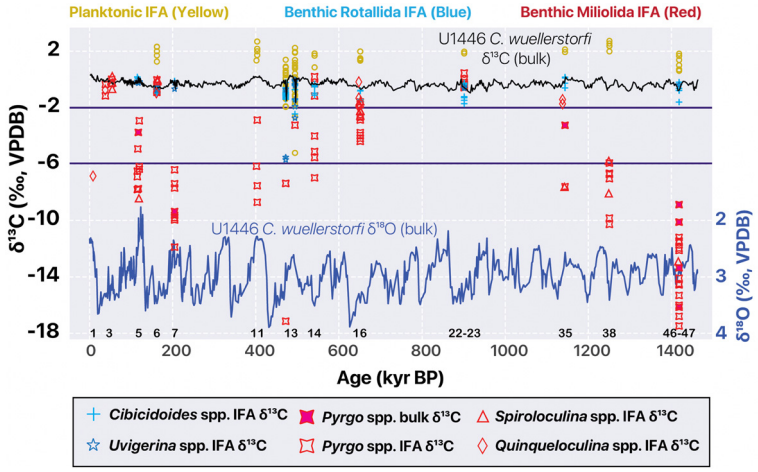

Fig. 7. U1446 IFA δ^{13}C with time series of bulk planktonic δ^{13}C and benthic δ^{18}O shown for context. Solid symbols are bulk Pyrgo analyses (250–355 μm; 2 to 6 individuals) for comparison with >355 μm IFA. Marine isotopic stages are numbered at the bottom (odd numbers indicate interglacial stages, even numbers indicate glacial stages). Solid horizontal line at −2‰ indicates δ^{13}C threshold for designating values as anomalously low. Solid horizontal line at −6‰ indicates the lowest benthic δ^{13}C documented in live benthic foraminifera at modern methane seeps.

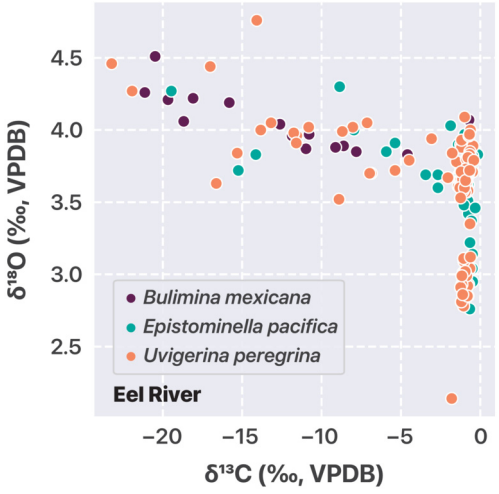

Fig. 8. Eel River IFA after Day (2003) indicating anomalous δ^{13}C recorded by all species analyzed.

combined with hydrate dissociation that briefly raises the SMTZ to within centimeters of the seafloor. Such transient excursions of the SMTZ may account for the incorporation of the anomalous δ^{13}C signal recorded by deep infaunal Miliolid genera but not by other shallower-dwelling infaunal (*Uvigerina* spp.) and epifaunal (*Cibicidoides* spp.) genera as follows.

5.2.1. Metabolic incorporation

A number of researchers have documented anomalous δ^{13}C values in living benthic foraminifera at methane hydrate-influenced locations, with values as low as −5.6‰ to −6‰ (Bernhard et al., 2010; Hill et al., 2004; Panieri and Sen Gupta, 2008; Sen Gupta et al., 1997). Possible explanations include direct incorporation of methane-influenced DIC during biomineralization (Panieri et al., 2014; Panieri and Sen Gupta, 2008; Rathburn et al., 2003) as well as grazing on methanogenic bacteria or endosymbiotic relationships with methanogenic bacteria (Bernhard et al., 2018; Hill et al., 2004; Panieri, 2006; Rathburn et al., 2003; Torres et al., 2003). We take these as possible explanations for the anomalous δ^{13}C values of the fossil Miliolid genera at U1446, accounting for values as low as ∼ −6‰. At the same time, however, there is a great deal of evidence that MDAC overgrowth can also account for the entire range of anomalously low benthic δ^{13}C tests observed at hydrate-influenced sites, to −16.9‰ (Panieri et al., 2017; Schneider et al., 2017) and lower.

5.2.2. MDAC overgrowth

Panieri et al. (2017) demonstrate that foraminiferal test structure and MDAC are structurally indistinguishable, with the same crystallographic orientation at the point of contact within the studied benthic tests (*Nonionella labradorica* and *Melonis barleeanus*). They suggest that these similarities yield a 'template' for initialization of authigenic carbonate precipitation. One possible explanation for our observations is that the Miliolida are particularly good templates, recording hydrate dissociation and the presence of the SMTZ not recorded by other benthic or planktonic species in the same samples.

The test structure of calcifying foraminifera is comprised of two groups, miliolid and hyaline. Miliolids precipitate calcite in the form of 2 to 3-micron long needles within cytoplasmic vesicles, with the calcite having high Mg/Ca similar to that precipitated inorganically from seawater {(de Nooijer et al., 2009; Sadekov et al., 2014) and references therein}. The needles are exported from the vesicles and assembled within an organic matrix, forming a new chamber; the arrangement of the needles provide the opaque 'porcelaneous' look to miliolid foraminifera. We suggest that the high Mg calcite of miliolid tests (Sadekov et al., 2014) provide such templates for overgrowth of MDAC, also enriched in Mg (Schneider et al., 2017). Unlike other species that may perish with exposure to the SMTZ environment, the deep infaunal Miliolida may continue to calcify for some time after the initiation of dissociation events and through short, transient, incursions of the SMTZ to near the sediment-water interface, accounting for test δ^{13}C values as low as ∼ −6‰, as documented at modern sites; by living beneath bacterial mats, directly incorporating methane-influenced DIC during biomineralization, grazing on methanogenic bacteria, or endosymbiotic relationships with methanogenic bacteria. Longer incursions of the SMTZ, to within a few cm of the seafloor, may also kill the deep infaunal Miliolida, providing ideal microenvironments for MDAC to precipitate within the relatively pristine chamber interior (the 'template' effect) but not within the already clay-filled chambers of other species, accounting for the very low values (−17‰) found in the Miliolida genera.

The lack of overprinting on other shallow infaunal benthic species and planktonic species within the same samples is inferred to indicate that additional post-burial MDAC overprinting (as in MIS 13) has not impacted these samples. In this case, the timing of

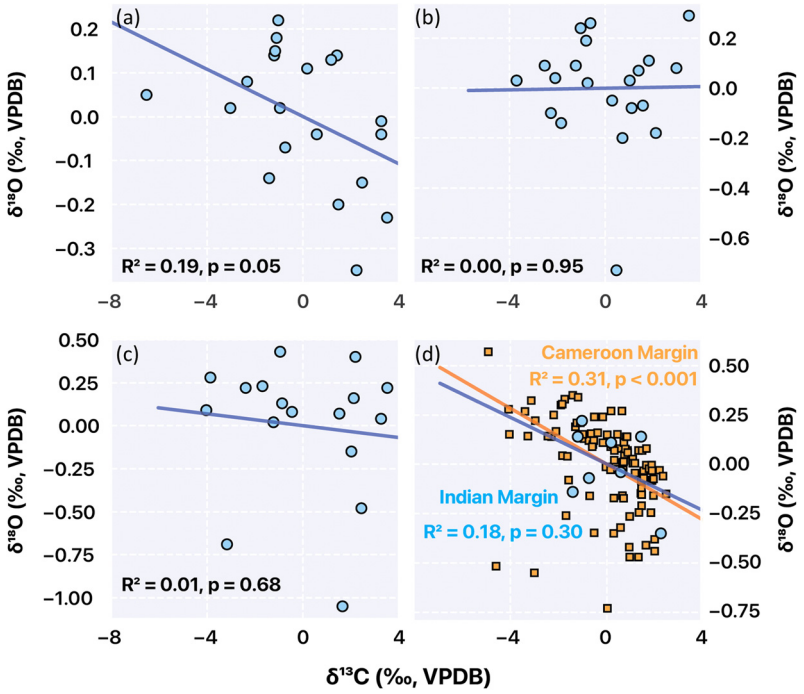

Fig. 9. IFA $\delta^{13}C$ vs $\delta^{18}O$ for samples with anomalously low $\delta^{13}C$. U1446 *Pyrgo spp.* IFA separated into (a) interglacial-, (b) glacial-, and (c) transitional-age intervals. (d) MIS 5e comparison of *Pyrgo* spp. from Indian margin Site U1446 and *Uvigerina peregrina* from Cameroon margin core MD2707 (Weldeab et al., 2022). In all cases, the sample mean has been subtracted from each IFA such that glacial-interglacial trends in seawater isotopic composition have been removed.

the anomalous $\delta^{13}C$ signal is imparted near the time of deposition and is close to the stratigraphic age.

5.3. Methane hydrate dissociation during interglacial intervals

Our sampling of this site is not a comprehensive survey of the sedimentary section nor of the samples available from the section, consisting of ~2 ky (30 cm) average sample spacing. Nevertheless, thirteen of the fifteen interglacial samples, three of the four glacial samples, and one of the two transitional samples investigated have anomalously low Miliolida $\delta^{13}C$, inferred to indicate hydrate dissociation. This is in comparison to the two proximal NGHP-01-18 and −19 sites combined, where only three events were identified on the basis of authigenic carbonate nodules (Teichert et al., 2014). Hence, we suggest that Miliolida $\delta^{13}C$ is a potentially sensitive indicator that may detect shorter transient upward excursions of the SMTZ that are insufficient to create authigenic carbonate crusts and develop macro-biological communities. We find that dissociation events are relatively common in the past, especially during interglacial intervals.

The slope of the IFA $\delta^{13}C$ versus $\delta^{18}O$ relationship can be used as an indicator of methane dissociation. Dissociation of methane hydrate leads to an increase in pore fluid $\delta^{18}O$ coincident with a decrease in pore fluid $\delta^{13}C$ (Davidson et al., 1983). Anomalous *Pyrgo* spp. are sufficiently abundant for this assessment during interglacial intervals (MIS 5, 7, 11, and 13), glacial intervals (14, 16, and 38), and transitional interval MIS 46-47 (Fig. 9a-c). While anomalously low $\delta^{13}C$ *Pyrgo* are abundant in all three climate states, only the interglacial samples show a significant negative correlation ($p = .05$). This suggests that the slope is not as sensitive an indicator of hydrate dissociation compared to test $\delta^{13}C$, possibly due to climate-induced variation of seawater ^{18}O. The slope of interglacial-age samples may be stronger because hydrate dissociation adds ^{18}O-enriched waters to ^{18}O depleted interglacial waters whereas dissociation adds ^{18}O enriched waters to progressively more ^{18}O-enriched transitional- and glacial-age waters, reducing the magnitude of the slope.

Additional $\delta^{13}C$ versus $\delta^{18}O$ evidence in support of *Pyrgo* recording hydrate dissociation events is that our MIS 5e *Pyrgo* IFA data from the Indian margin is very similar to that measured for MIS 5e *Uvigerina peregrina* IFA data from the Cameroon margin, western equatorial Africa (Fig. 9d). Modern methane hydrates on this margin exist as disseminated nodules in muddy sediments within 1.4 m to 3 m below the sea floor and as massive hydrates 5 m to 6 m below the sea floor (Weldeab et al., 2022). Here, the MIS 5e dissociation event is inferred to have resulted from a 3 °C to 5 °C warming of bottom waters at the core site (MD2707; 1295 mbsl) in response to weakening of Atlantic meridional overturning circulation (AMOC). *U. peregrina* $\delta^{13}C$ IFA anomalies reached −8.7‰ and are interpreted to largely reflect metabolic incorporation; post-depositional diagenetic overprinting was ruled out by SEM and mass balance considerations. It is not clear why *U. peregrina* records anomalous $\delta^{13}C$ on the Cameroon margin but not the Indian margin.

Intermediate water temperature changes can potentially modulate dissociation and subsequent incorporation of anomalous $\delta^{13}C$ into foraminiferal tests on the Indian Margin, similar to the Cameroon margin. Ma et al. (2019) examined benthic foraminifera $\delta^{18}O$, $\delta^{13}C$, foraminiferal assemblage, and benthic-planktonic ^{14}C age offsets in the northern Bay of Bengal to reconstruct changes in intermediate water circulation from the last glacial maximum to the Holocene. Glacial intervals are characterized by reduced production of relatively warm Red Sea Water, Persian Gulf Water, and Indonesian Intermediate Water, all of which contribute to the relatively warm modern Bay of Bengal Intermediate Water. Ma et al. (2019) conclude that, during glacial intervals, northern Bay of Bengal intermediate waters are characterized by increased contributions from colder southern sourced water, including Circumpolar Deep Water and North Atlantic Deep Water. They estimate that the temperature of the intermediate water (1375 m) is 3 to 4 °C warmer in the Holocene compared to the LGM. Such warmer temperatures would favor hydrate dissociation during interglacial intervals (Buffett and Archer, 2004; Mazumdar et al., 2014) promoting upward migration of the SMTZ and the associated $\delta^{13}C_{DIC}$

gradient toward the sediment-water interface (Ruppel and Waite, 2020), accounting for the observed $\delta^{13}C$ anomalies. Dissociation events during glacial intervals may be attributed to drops in sea level {e.g. (Mazumdar et al., 2014; Ruppel and Kessler, 2017)}.

6. Conclusions

Methane dissociation is inferred for glacial, transitional, and interglacial intervals on the basis of anomalously low benthic $\delta^{13}C$ in the Mahanadi offshore basin, northwest Bay of Bengal (Site U1446). A negative correlation between $\delta^{13}C$ and $\delta^{18}O$ during interglacial intervals is interpreted as supporting this interpretation, with dissociation modulated by increased intermediate water temperature.

At U1446, anomalously low $\delta^{13}C$ values in the majority of samples are unique to Miliolida benthic foraminifera *Pyrgo* spp., *Spiroloculina* spp., and *Quinqueloculina* spp. Such anomalies are not found in other benthic or planktonic species in the same samples nor at the non-hydrate-influenced control sites. This suggests that species within these genera are sensitive recorders of methane hydrate dissociation events on the northeast Indian margin, and can detect short, transient dissociation activity that is insufficient to create authigenic carbonate crusts and macro-biological communities at the sediment-water interface.

On the basis of previous work at hydrate-influenced sites, anomalous $\delta^{13}C$ as low as approximately $-6‰$ may have been incorporated metabolically via biomineralization of methane-influenced DIC, feeding on methanogenic bacteria, or endosymbiotic relationships with methanogenic bacteria. Alternatively, MDAC overgrowth can account for the entire range of anomalous values observed (to $-17.5‰$); we have not distinguished between these possibilities.

Only the three Miliolida genera were impacted in 9 of the 11 marine isotopic stages where anomalously low $\delta^{13}C$ values were documented (MIS 1, 5, 7, 11, 14, 16, 35, 38, and 46–47); other benthic and planktonic species from the same 2 cm thick samples (~70 to 150 years duration) were not anomalous. On this basis, we infer that the signal was imparted to deep infaunal individuals close to the time of deposition, at times when the SMTZ transiently shoaled to near the sediment-water interface, without subsequent modification thereafter. In contrast, the two MIS 13 samples in which all species analyzed (planktonic and benthic) contained individuals with anomalously low $\delta^{13}C$ are interpreted as having experienced one, or more, episodes of MDAC overprinting since being deposited, during prolonged exposure within the SMTZ.

CRediT authorship contribution statement

S.C. Clemens: Conceptualization, methodology, isotopic analysis, interpretation, writing, original draft. **K. Thirumalai:** Conceptualization, methodology, isotopic analysis, interpretation, review and editing. **D. Oppo:** Methodology, interpretation, review and editing.

Declaration of competing interest

The authors declare that they have no known competing financial interests or personal relationships that could have appeared to influence the work reported in this paper.

Data availability

All data is included in Table S1.

Acknowledgements

This research used samples provided by the Integrated Ocean Drilling Program (IODP).

This research was supported by National Science Foundation OCE1634774 to S.C. The manuscript was substantially improved by the constructive criticism and suggestions of Editor L. Coogan and two anonymous reviewers. The suggestion to evaluate additional Miliolida genera was particularly valuable.

Appendix A. Supplementary material

Supplementary material related to this article can be found online at https://doi.org/10.1016/j.epsl.2023.118101.

References

Åström, E.K.L., Sen, A., Carroll, M.L., Carroll, J., 2020. Cold seeps in a warming Arctic: insights for Benthic ecology. Front. Mar. Sci. 7, 244.

Babineaux, G., Oppo, D., Powers, N., Thirumalai, K., Selznick, E., Panieri, G., Macelloni, L., 2021. New analyses reveal a high variability of methane release over the last 50 kys at Woolsey Mound (Gulf of Mexico). In: AGU Fall Meeting New Orleans.

Bernhard, J.M., Martin, J.B., Rathburn, A.E., 2010. Combined carbonate carbon isotopic and cellular ultrastructural studies of individual benthic foraminifera: 2. Toward an understanding of apparent disequilibrium in hydrocarbon seeps. Paleoceanography 25.

Bernhard, J.M., Tsuchiya, M., Nomaki, H., 2018. Ultrastructural observations on prokaryotic associates of benthic foraminifera: food, mutualistic symbionts, or parasites? Mar. Micropaleontol. 138, 33–45.

Bolton, C.T., Chang, L., Clemens, S.C., Kodama, K., Ikehara, M., Medina-Elizalde, M., Paterson, G.A., Roberts, A.P., Rohling, E.J., Yamamoto, Y., Zhao, X., 2013. A 500,000 year record of Indian summer monsoon dynamics recorded by eastern equatorial Indian Ocean upper water-column structure. Quat. Sci. Rev. 77, 167–180.

Brown, A., 2011. Interpretation of Three-Dimensional Seismic Data, 7 ed. AAPG & SEG.

Buffett, B., Archer, D., 2004. Global inventory of methane clathrate: sensitivity to changes in the deep ocean. Earth Planet. Sci. Lett. 227, 185–199.

Buzas, M.A., Culver, S.J., Jorissen, F.J., 1993. A statistical evaluation of the microhabitats of living (stained) infaunal benthic foraminifera. Mar. Micropaleontol. 20, 311–320.

Capozzi, R., Guido, F.L., Oppo, D., Gabbianelli, G., 2012. Methane-derived authigenic carbonates (MDAC) in northern-central Adriatic Sea: relationships between reservoir and methane seepages. Mar. Geol. 332–334, 174–188.

Clemens, S.C., Kuhnt, W., LeVay, L.J., Anand, P., Ando, T., Bartol, M., Bolton, C.T., Ding, X., Gariboldi, K., Giosan, L., Hathorne, E.C., Huang, Y., Jaiswal, P., Kim, S., Kirkpatrick, J.B., Littler, K., Marino, G., Martinez, P., Naik, D., Peketi, A., Phillips, S.C., Robinson, M.M., Romero, O.E., Sagar, N., Taladay, K.B., Taylor, S.N., Thirumalai, K., Uramoto, G., Usui, Y., Wang, J., Yamamoto, M., Zhou, L., 2016a. Site U1443. In: Clemens, S.C., Kuhnt, W., LeVay, L.J., Scientists, t.E. (Eds.), Indian Monsoon Rainfall. International Ocean Discovery Program. College Station, TX.

Clemens, S.C., Kuhnt, W., LeVay, L.J., Anand, P., Ando, T., Bartol, M., Bolton, C.T., Ding, X., Gariboldi, K., Giosan, L., Hathorne, E.C., Huang, Y., Jaiswal, P., Kim, S., Kirkpatrick, J.B., Littler, K., Marino, G., Martinez, P., Naik, D., Peketi, A., Phillips, S.C., Robinson, M.M., Romero, O.E., Sagar, N., Taladay, K.B., Taylor, S.N., Thirumalai, K., Uramoto, G., Usui, Y., Wang, J., Yamamoto, M., Zhou, L., 2016b. Site U1446. In: Clemens, S.C., Kuhnt, W., LeVay, L.J., Scientists, t.E. (Eds.), Indian Monsoon Rainfall. International Ocean Discovery Program. College Station, TX.

Clemens, S.C., Murray, D.W., Prell, W.L., 1996. Nonstationary phase of the Plio-Pleistocene Asian Monsoon. Science 274, 943–948.

Clemens, S.C., Yamamoto, M., Thirumalai, K., Giosan, L., Richey, J.N., Nilsson-Kerr, K., Rosenthal, Y., Anand, P., McGrath, S.M., 2021. Remote and local drivers of Pleistocene South Asian summer monsoon precipitation: a test for future predictions. Sci. Adv. 7, eabg3848.

Collett, T., Riedel, M., Cochran, J., Boswell, R., Presley, J., Kumar, P., Sathe, A., Sethi, A., Lall, M., Sibal, V., Scientists, a.t.N.E., 2015. Indian national gas hydrate program expedition 01 report. In: Survey, U.S.G. (Ed.). U.S. Geological Survey, p. 1442.

Collett, T.S., Boswell, R., Cochran, J.R., Kumar, P., Lall, M., Mazumdar, A., Ramana, M.V., Ramprasad, T., Riedel, M., Sain, K., Sathe, A.V., Vishwanath, K., 2014. Geologic implications of gas hydrates in the offshore of India: results of the national gas hydrate program expedition 01. Mar. Pet. Geol. 58, 3–28.

Crutchley, G.J., Berndt, C., Geiger, S., Klaeschen, D., Papenberg, C., Klaucke, I., Hornbach, M.J., Bangs, N.L.B., Maier, C., 2013. Drivers of focused fluid flow and methane seepage at South Hydrate Ridge, offshore Oregon, USA. Geology 41, 551–554.

Davidson, D.W., Leaist, D.G., Hesse, R., 1983. Oxygen-18 enrichment in the water of a clathrate hydrate. Geochim. Cosmochim. Acta 47, 2293–2295.

Day, S.A., 2003. Documenting Modern and Ancient Methane Release from Cold Seeps Using Deep-Sea Benthic Foraminifera, Geological Sciences. University of Florida. University of Florida.

de Nooijer, L.J., Toyofuku, T., Kitazato, H., 2009. Foraminifera promote calcification by elevating their intracellular pH. Proc. Natl. Acad. Sci. 106, 15374–15378.

Dickens, G.R., Fewless, T., Thomas, E., Bralower, T., Gingerich, L., Schmitz, P., 2003. Excess barite accumulation during the Paleocene-Eocene thermal maximum: massive input of dissolved barium from seafloor gas hydrate reservoirs. Spec. Pap., Geol. Soc. Am. 369.

Dickens, G.R., O'Neil, J.R., Rea, D.K., Owen, R.M., 1995. Dissociation of oceanic methane hydrate as a cause of the carbon isotope excursion at the end of the Paleocene. Paleoceanography 10, 965–971.

Enge, A.J., Kucera, M., Heinz, P., 2012. Diversity and microhabitats of living benthic foraminifera in the abyssal Northeast Pacific. Mar. Micropaleontol. 96–97, 84–104.

Fang, Y., Wei, J., Lu, H., Liang, J., Lu, J.a, Fu, J., Cao, J., 2019. Chemical and structural characteristics of gas hydrates from the Haima cold seeps in the Qiongdongnan Basin of the South China Sea. J. Asian Earth Sci. 182, 103924.

Gieskes, J., Rathburn, A.E., Martin, J.B., Pérez, M.E., Mahn, C., Bernhard, J.M., Day, S., 2011. Cold seeps in Monterey Bay, California: geochemistry of pore waters and relationship to benthic foraminiferal calcite. Appl. Geochem. 26, 738–746.

Gooday, A.J., Malzone, M.G., Bett, B.J., Lamont, P.A., 2010. Decadal-scale changes in shallow-infaunal foraminiferal assemblages at the Porcupine Abyssal Plain, NE Atlantic. Deep-Sea Res., Part 2, Top. Stud. Oceanogr. 57, 1362–1382.

Hanson, R.S., Hanson, T.E., 1996. Methanotrophic bacteria. Microbiol. Rev. 60, 439–471.

Hill, T.M., Kennett, J.P., Spero, H.J., 2003. Foraminifera as indicators of methane-rich environments: a study of modern methane seeps in Santa Barbara Channel, California. Mar. Micropaleontol. 49, 123–138.

Hill, T.M., Kennett, J.P., Valentine, D.L., 2004. Isotopic evidence for the incorporation of methane-derived carbon into foraminifera from modern methane seeps, Hydrate Ridge, Northeast Pacific. Geochim. Cosmochim. Acta 68, 4619–4627.

IPCC, 2021. Climate Change 2021: the Physical Science Basis. Contribution of Working Group I to the Sixth Assessment Report of the Intergovernmental Panel on Climate Change (IPCC 2021).

James, R.H., Bousquet, P., Bussmann, I., Haeckel, M., Kipfer, R., Leifer, I., Niemann, H., Ostrovsky, I., Piskozub, J., Rehder, G., Treude, T., Vielstädte, L., Greinert, J., 2016. Effects of climate change on methane emissions from seafloor sediments in the Arctic Ocean: a review. Limnol. Oceanogr. 61, S283–S299.

Johnson, J.E., Phillips, S.C., Torres, M.E., Piñero, E., Rose, K.K., Giosan, L., 2014. Influence of total organic carbon deposition on the inventory of gas hydrate in the Indian continental margins. Mar. Pet. Geol. 58, 406–424.

Joshi, R.K., Mazumdar, A., Peketi, A., Ramamurty, P.B., Naik, B.G., Kocherla, M., Carvalho, M.A., Mahalakshmi, P., Dewangan, P., Ramana, M.V., 2014. Gas hydrate destabilization and methane release events in the Krishna–Godavari Basin, Bay of Bengal. Mar. Pet. Geol. 58, 476–489.

Joye, S.B., 2020. The geology and biogeochemistry of hydrocarbon seeps. Annu. Rev. Earth Planet. Sci. 48, 205–231.

Keigwin, L.D., 2002. Late Pleistocene-Holocene Paleoceanography and ventilation of the Gulf of California. J. Oceanogr. 58, 421–432.

Kennett, J.P., Cannariato, K.G., Hendy, I.L., Behl, S.J., 2000. Carbon isotopic evidence for methane hydrate instability during quaternary interstadials. Science 288, 128–133.

Kim, B., Zhang, Y.G., 2022. Methane hydrate dissociation across the Oligocene–Miocene boundary. Nat. Geosci. 15, 203–209.

Klaucke, I., Weinrebe, W., Petersen, C.J., Bowden, D., 2010. Temporal variability of gas seeps offshore New Zealand: multi-frequency geoacoustic imaging of the Wairarapa area, Hikurangi margin. Mar. Geol. 272, 49–58.

Lein, A.Y., 2004. Authigenic carbonate formation in the ocean. Lithol. Miner. Resour. 39, 1–30.

Linke, P., Lutze, G.F., 1993. Microhabitat preferences of benthic foraminifera - static concept or a dynamic adaptation to optimize food acquisition? Mar. Micropaleontol. 20, 215–234.

Lobegeier, M.K., Sen Gupta, B.K., 2008. Foraminifera of hydrocarbon seeps, Gulf of Mexico. J. Foraminiferal Res. 38, 93–116.

Lorenson, T.D., Collett, T.S., 2018. National gas hydrate program expedition 01 offshore India; gas hydrate systems as revealed by hydrocarbon gas geochemistry. Mar. Pet. Geol. 92, 477–492.

Ma, G., Zhan, L., Lu, H., Hou, G., 2021. Structures in shallow marine sediments associated with gas and fluid migration. J. Mar. Sci. Eng. 9.

Ma, R., Sépulcre, S., Licari, L., Bassinot, F., Liu, Z., Tisnérat-Laborde, N., Kallel, N., Yu, Z., Colin, C., 2019. Changes in intermediate circulation in the Bay of Bengal since the last glacial maximum as inferred from Benthic Foraminifera assemblages and geochemical proxies. Geochem. Geophys. Geosyst. 20, 1592–1608.

Martin, J.B., Day, S.A., Rathburn, A.E., Perez, M.E., Mahn, C., Gieskes, J., 2004. Relationships between the stable isotopic signatures of living and fossil foraminifera in Monterey Bay, California. Geochem. Geophys. Geosyst. 5.

Mazumdar, A., Dewangan, P., Peketi, A., Gullapalli, S., Kalpana, M.S., Naik, G.P., Shetty, D., Pujari, S., Pillutla, S.P.K., Gaikwad, V.V., Nazareth, D., Sangodkar, N.S., Dakara, G., Kumar, A., Mishra, C.K., Singha, P., Reddy, R., 2018. The first record of active methane (cold) seep ecosystem associated with shallow methane hydrate from the Indian EEZ. J. Earth Syst. Sci. 128, 18.

Mazumdar, A., Peketi, A., Joao, H.M., Dewangan, P., Ramprasad, T., 2014. Pore-water chemistry of sediment cores off Mahanadi Basin, Bay of Bengal: possible link to deep seated methane hydrate deposit. Mar. Pet. Geol. 49, 162–175.

McCorkle, D.C., Keigwin, L.D., Corliss, B.H., Emerson, S.R., 1990. The influence of microhabitats on the carbon isotopic composition of deep sea benthic foraminifera. Paleoceanography 5, 161–185.

Melaniuk, K., Sztybor, K., Treude, T., Sommer, S., Rasmussen, T.L., 2022. Influence of methane seepage on isotopic signatures in living deep-sea benthic foraminifera, 79°N. Sci. Rep. 12, 1169.

Miller, D.J., Ketzer, J.M., Viana, A.R., Kowsmann, R.O., Freire, A.F.M., Oreiro, S.G., Augustin, A.H., Lourega, R.V., Rodrigues, L.F., Heemann, R., Preissler, A.G., Machado, C.X., Sbrissa, G.F., 2015. Natural gas hydrates in the Rio Grande Cone (Brazil): a new province in the western South Atlantic. Mar. Pet. Geol. 67, 187–196.

Mulitza, S., Bickert, T., Bostock, H.C., Chiessi, C.M., Donner, B., Govin, A., Harada, N., Huang, E., Johnstone, H., Kuhnert, H., Langner, M., Lamy, F., Lembke-Jene, L., Lisiecki, L., Lynch-Stieglitz, J., Max, L., Mohtadi, M., Mollenhauer, G., Muglia, J., Nürnberg, D., Paul, A., Rühlemann, C., Repschläger, J., Saraswat, R., Schmittner, A., Sikes, E.L., Spielhagen, R.F., Tiedemann, R., 2022. World atlas of late quaternary foraminiferal oxygen and carbon isotope ratios. Earth Syst. Sci. Data 14, 2553–2611.

Oppo, D., De Siena, L., Kemp, D.B., 2020. A record of seafloor methane seepage across the last 150 million years. Sci. Rep. 10, 2562.

Oppo, D., Evans, S., Iacopini, D., Kabir, S.M.M., Maselli, V., Jackson, C.A.L., 2021. Leaky salt: pipe trails record the history of cross-evaporite fluid escape in the northern Levant Basin, Eastern Mediterranean. Basin Res. 33, 1798–1819.

Oppo, D., Hovland, M., 2019. Role of deep-sourced fluids on the initiation and growth of isolated carbonate build-ups. Mar. Pet. Geol. 105, 141–157.

Panieri, G., 2006. Foraminiferal response to an active methane seep environment: a case study from the Adriatic Sea. Mar. Micropaleontol. 61, 116–130.

Panieri, G., Camerlenghi, A., Conti, S., Pini, G.A., Cacho, I., 2009. Methane seepages recorded in benthic foraminifera from Miocene seep carbonates, Northern Apennines (Italy). Palaeogeogr. Palaeoclimatol. Palaeoecol. 284, 271–282.

Panieri, G., Graves, C.A., James, R.H., 2016. Paleo-methane emissions recorded in foraminifera near the landward limit of the gas hydrate stability zone offshore western Svalbard. Geochem. Geophys. Geosyst.

Panieri, G., James, R.H., Camerlenghi, A., Westbrook, G.K., Consolaro, C., Cacho, I., Cesari, V., Cervera, C.S., 2014. Record of methane emissions from the West Svalbard continental margin during the last 23.500yrs revealed by δ13C of benthic foraminifera. Glob. Planet. Change 122, 151–160.

Panieri, G., Lepland, A., Whitehouse, M.J., Wirth, R., Raanes, M.P., James, R.H., Graves, C.A., Crémière, A., Schneider, A., 2017. Diagenetic Mg-calcite overgrowths on foraminiferal tests in the vicinity of methane seeps. Earth Planet. Sci. Lett. 458, 203–212.

Panieri, G., Sen Gupta, B.K., 2008. Benthic Foraminifera of the Blake Ridge hydrate mound, Western North Atlantic Ocean. Mar. Micropaleontol. 66, 91–102.

Peketi, A., Mazumdar, A., Pillutla, S.P.K., Patil, D.J., 2020. Influence of dual sulfate reduction pathways on pore-fluid chemistry and occurrences of methane hydrate in sediment cores (IODP-353) off Mahanadi basin, Bay of Bengal. Geochem. J. 54, 1–11.

Pierce, J., Weissel, J., 1989. Shipboard scientific party. Site 758. In: Pierce, J., Weissel, J. (Eds.), Proc. ODP, Init. Repts. Ocean Drilling Program. College Station, TX, pp. 359–453.

Portilho-Ramos, R.C., Cruz, A.P.S., Barbosa, C.F., Rathburn, A.E., Mulitza, S., Venancio, I.M., Schwenk, T., Rühlemann, C., Vidal, L., Chiessi, C.M., Silveira, C.S., 2018. Methane release from the southern Brazilian margin during the last glacial. Sci. Rep. 8, 5948.

Prell, W.L., Niitsuma, N., Party, S.S., 1989. Site 722. In: Prell, W.L., Niitsuma, H. (Eds.), Ocean Drill. Program Init. Repts. Ocean Drilling Program. College Station, pp. 255–318.

Rathburn, A.E., Pérez, M.E., Martin, J.B., Day, S.A., Mahn, C., Gieskes, J., Ziebis, W., Williams, D., Bahls, A., 2003. Relationships between the distribution and stable isotopic composition of living benthic foraminifera and cold methane seep biogeochemistry in Monterey Bay, California. Geochem. Geophys. Geosyst. 4.

Robinson, C.A., Bernhard, J.M., Levin, L.A., Mendoza, G.F., Blanks, J.K., 2004. Surficial hydrocarbon seep Infauna from the blake ridge (Atlantic Ocean, 2150 m) and the Gulf of Mexico (690–2240 m). Mar. Ecol. 25, 313–336.

Ruppel, C.D., Kessler, J.D., 2017. The interaction of climate change and methane hydrates. Rev. Geophys. 55, 126–168.

Ruppel, C.D., Waite, W.F., 2020. Timescales and processes of methane hydrate formation and breakdown, with application to geologic systems. J. Geophys. Res., Solid Earth 125, e2018JB016459.

Sadekov, A.Y., Bush, F., Kerr, J., Ganeshram, R., Elderfield, H., 2014. Mg/Ca composition of benthic foraminifera Miliolacea as a new tool of paleoceanography. Paleoceanography, 2014PA002654.

Sasaki, T., Warén, A., Kano, Y., Okutani, T., Fujikura, K., 2010. Gastropods from recent hot vents and cold seeps: systematics. Divers. Life Strat., 169–254.

Sassen, R., Roberts, H.H., Aharon, P., Larkin, J., Chinn, E.W., Carney, R., 1993. Chemosynthetic bacterial mats at cold hydrocarbon seeps, Gulf of Mexico continental slope. Org. Geochem. 20, 77–89.

Schneider, A., Crémière, A., Panieri, G., Lepland, A., Knies, J., 2017. Diagenetic alteration of benthic foraminifera from a methane seep site on Vestnesa Ridge (NW Svalbard). Deep-Sea Res., Part 1, Oceanogr. Res. Pap. 123, 22–34.

Sen Gupta, B.K., Platon, E., Bernhard, J.M., Aharon, P., 1997. Foraminiferal colonization of hydrocarbon-seep bacterial mats and underlying sediment, Gulf of Mexico slope. J. Foraminiferal Res. 27, 292–300.

Sibuet, M., Roy, K.O.-L., 2003. Cold seep communities on continental margins: structure and quantitative distribution relative to geological and fluid venting patterns. In: Wefer, G., Billett, D., Hebbeln, D., Jørgensen, B.B., Schlüter, M., van Weering, T.C.E. (Eds.), Ocean Margin Systems. Springer Berlin Heidelberg, Berlin, Heidelberg, pp. 235–251.

Teichert, B.M.A., Johnson, J.E., Solomon, E.A., Giosan, L., Rose, K., Kocherla, M., Connolly, E.C., Torres, M.E., 2014. Composition and origin of authigenic carbonates in the Krishna–Godavari and Mahanadi Basins, eastern continental margin of India. Mar. Pet. Geol. 58, 438–460.

Thirumalai, K., Clemens, S.C., Partin, J.W., 2020. Methane, monsoons, and modulation of millennial-scale climate. Geophys. Res. Lett. 47, e2020GL087613.

Torres, M.E., Martin, R.A., Klinkhammer, G.P., Nesbitt, E.A., 2010. Post depositional alteration of foraminiferal shells in cold seep settings: new insights from flow-through time-resolved analyses of biogenic and inorganic seep carbonates. Earth Planet. Sci. Lett. 299, 10–22.

Torres, M.E., Mix, A.C., Kinports, K., Haley, B., Klinkhammer, G.P., McManus, J., de Angelis, M.A., 2003. Is methane venting at the seafloor recorded by δ^{13}C of benthic foraminifera shells? Paleoceanography 18.

Ussler, W., Paull, C.K., 2008. Rates of anaerobic oxidation of methane and authigenic carbonate mineralization in methane-rich deep-sea sediments inferred from models and geochemical profiles. Earth Planet. Sci. Lett. 266, 271–287.

Wan, S., Feng, D., Chen, F., Zhuang, C., Chen, D., 2018. Foraminifera from gas hydrate-bearing sediments of the northeastern South China Sea: proxy evaluation and application for methane release activity. J. Asian Earth Sci. 168, 125–136.

Wang, M., Li, Q., Cai, F., Liang, J., Yan, G., Wang, Z., Sun, Y., Luo, D., Dong, G., Cao, Y., 2019. Formation of authigenic carbonates at a methane seep site in the middle Okinawa Trough, East China Sea. J. Asian Earth Sci. 185, 104028.

Weldeab, S., Schneider, R.R., Yu, J., Kylander-Clark, A., 2022. Evidence for massive methane hydrate destabilization during the penultimate interglacial warming. Proc. Natl. Acad. Sci. 119, e2201871119.

Whiticar, M.J., 1999. Carbon and hydrogen isotope systematics of bacterial formation and oxidation of methane. Chem. Geol. 161, 291–314.

You, K., Flemings, P.B., Malinverno, A., Collett, T.S., Darnell, K., 2019. Mechanisms of methane hydrate formation in geological systems. Rev. Geophys. 57, 1146–1196.

Zhou, Y., Di, P., Li, N., Chen, F., Su, X., Zhang, J., 2020. Unique authigenic mineral assemblages and planktonic foraminifera reveal dynamic cold seepage in the Southern South China Sea. Minerals 10.